RSC Advances

PAPER

View Article Online
View Journal | View Issue

Cite this: *RSC Adv.*, 2019, **9**, 6542

Kinetic study on the grain growth of PuO_2 nanocrystals†

Daniel Bouëxière, Karin Popa, Olaf Walter * and Marco Cologna

Received 20th December 2018
Accepted 18th February 2019

DOI: 10.1039/c8ra10430a

rsc.li/rsc-advances

Kinetic measurements on the grain growth of PuO_2 nano-crystals are presented. On the basis of isothermal XRD measurements at temperatures of 820 °C, 900 °C, 1000 °C, and 1100 °C the activation energy for the crystallite growth of PuO_2 nanopowder is determined as 351(5) kJ mol^{-1} in the temperature range from 820 to 1000 °C. Modelling shows that in this T range growth happens likely through surface diffusion.

1 Introduction

The standard fuel for current commercial nuclear reactors is based on actinide dioxides: UO_2 or UO_2–PuO_2 mixed oxides (MOX). The properties of actinide dioxide nanocrystals are of interest for various stages of the nuclear fuel cycle. For example, nanostructures of actinide dioxides are formed in the high burn-up structure of spent fuel.[1] During the past ten years, the Joint Research Centre (JRC) has built-up expertise in the formation and characterisation of actinide dioxide nano-particles.[1–6] More recently the actinide oxalates were used as the starting material for the synthesis of actinide dioxide nano-powders *via* thermal treatment.[7–10] The oxalate route offers several advantages: it is often applied in the nuclear fuel cycle and therefore is state of the art in separation,[11] recycling of the actinide ions,[12] fuel production[13] or the reprocessing of spent fuel.[14,15] The main differences between the wet and the dry oxalate decomposition are the lower temperature and the formation of spherical particles for the wet oxalate decomposition,[8–10] whereas the powders resulting from the dry decomposition maintain the platelet shape of the original oxalate.[7] The bulk modulus of spherical UO_2 nano-particles obtained by thermal decomposition of inorganic media[2] was measured to be 50% lower compared to the bulk.[16] The nanometric dimension of the particles enables as well to follow the growth of the crystallite as a function of the temperature by high-temperature X-ray diffraction (HT-XRD). So it was found that the crystallite growth rate of AnO_2 powders increases in the order Th, Np, Pu, U, suggesting that the sintering ability should follow the same trend.[10] A quantitative model was not obtained yet. Here we will close this knowledge gap by presenting for the first time kinetic data on the crystallite size growth of nano-sized PuO_2 powders. The data are interpreted with a simplified model, which allows the activation energy determination to 351 kJ mol^{-1} for the growth of PuO_2 nanograins in the temperature range (820–1000 °C).

2 Experimental

All work has been carried out in the laboratories of the JRC Karlsruhe licensed for handling plutonium, with respect to the German radioprotection regulations. The heart of the work presented here are high-temperature (HT) XRD measurements performed during isothermal annealing at temperatures of 820 °C, 900 °C, 1000 °C, and 1100 °C.

2.1 Synthesis

The nanocrystalline PuO_2 powder used in this study has been synthesised using the newly implemented oxalate decomposition method in hot compressed water.[8–10] In short, a 0.8 molar (M) Pu^{IV} solution in 4 M HNO_3 has been directly precipitated with oxalic acid (10% excess) as $Pu(C_2O_4)_2 \cdot 6H_2O$. The precipitate was washed several times with distilled water in order to remove any trace of nitrate and 100 mg Pu-oxalate hexahydrate were placed in a 10 ml Teflon reactor together with 5 ml distilled water. The hydrothermal decomposition was conducted for 120 h at 95 °C under autogenic pressure (1–2 bar). Powder XRD characterisation was performed on a Bruker D8 diffractometer equipped with a LinxEye position sensitive detector, of which the Rietveld refinement lead to $R_{profile}$ of 1.8% and $R_{weighted}$ of 3.0%. For the results of the Rietveld analyses refer to the ESI; in Fig. S1† is presented the result from the Rietveld analyses of the original PuO_2 nano powders. Fig. S2† is the result of the Rietveld analysis of the same PuO_2 nano powder on the high temperature Pt sample holder. Fig. S3† shows the diffractogram of sample on the high temperature Pt sample holder at the end of measurements.

The Rietveld analysis of the PuO_2 obtained by the hydrothermal decomposition of Pu-oxalate hexahydrate confirms the nanometric nature of the PuO_2 (cubic fluorite structure, cubic $Fm\bar{3}m$ (225) space group) with a particle size of 3.7 ± 1.0 nm and a lattice parameter of 5.4042(2) Å (Fig. S1†). The nanocrystals form almost spherical agglomerates with a typical size of 100–200 nm.

European Commission, DG Joint Research Centre, JRC-Karlsruhe, P. O. Box 2340, 76125 Karlsruhe, Germany. E-mail: olaf.walter@ec.europa.eu

† Electronic supplementary information (ESI) available. See DOI: 10.1039/c8ra10430a

2.2 Microscopic characterisation

Transmission electron microscope (TEM) analyses were performed on a TecnaiG2 (FEI™) 200 kV microscope equipped with field emission gun. The samples for the TEM investigations were prepared by dropping samples suspended in acetone on a TEM grid and evaporating the solvent. Statistical evaluation of the particle size of the initially synthesized PuO_2 nano particles revealed a mean size of 2.6 ± 0.5 nm in agreement with the size of 3.7 ± 1.0 nm calculated from the broadening of the XRD peaks.[8]

A Philips XL40 Scanning Electron Microscope (SEM) equipped with Energy Dispersive X-ray Spectroscopy (EDS) was used. The sample grains were deposited on a carbon sticker and covered with carbon to avoid charging.

2.3 High-temperature XRD measurements and calculation of crystallite size

For HT-XRD measurements (up to 1100 °C), all the data were collected under vacuum on a Bruker D8 diffractometer mounted in a Bragg–Brentano configuration with a curved Ge (1,1,1) monochromator, a ceramic copper tube (40 kV, 40 mA), equipped with an Anton Paar HTK 2000 chamber.

Two sets of experiments were conducted. First, in order to define the temperature range for the isothermal experiments, a diffractogram with a large 2θ window ($20° < 2\theta < 120°$) was taken in the 500–900 °C range (Fig. 1). Each measurement took 3 hours. On the base of this study, the temperature range for the isothermal annealing was set in the 820–1200 °C interval, in the range $45° < 2\theta < 60°$, where three diffraction peaks of PuO_2 are present. This window was chosen to perform the time dependent measurements on the changes of the line broadening within a reasonable amount of time (36 min). The powder was heated in the HT-XRD device with a rate of 10 °C min^{-1} to 820 °C, held for 30 h, and successively heated further to 900 °C, 1000 °C, 1100 °C and 1200 °C, following the same measurement procedure.

Before performing the high-temperature XRD measurements with a reduced 2θ range, a full diffractogram was taken in the range $20° < 2\theta < 120°$ at room temperature on the Pt sample holder of the HT X-ray diffractometer. A Rietveld refinement (Highscore plus) was performed, leading to $R_{profile}$ of 6.5% and $R_{weighted}$ of 9.0% based on two phases (the Pt sample holder and PuO_2, more details see ESI, Fig. S2†). A diffractogram under identical conditions was registered at the end of the series of the measurement showing clearly the changes in the particle size (Fig. S3, ESI†).

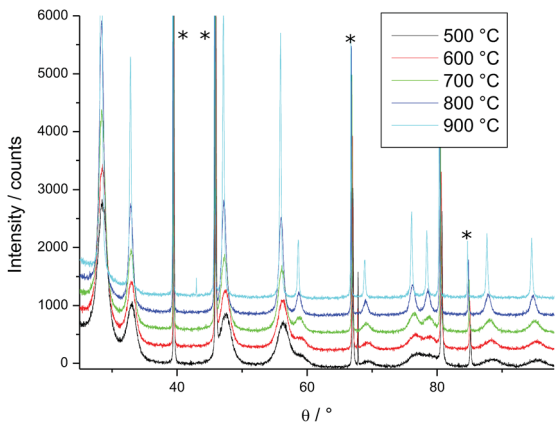

Fig. 1 Variation of the XRD patterns of PuO_2 as a function of temperature; peaks marked by * arise from the sample holder.

However, the crystallite size (D) during the high temperature isotherms were calculated as the average from the three peaks appearing in the range $45° < 2\theta < 60°$ after profile fitting by measuring independently the line broadening at half the maximum intensity (FWHM) for each Bragg angle and the applying the Scherrer equation (Eq. (1)):

$$D = \frac{k\lambda}{\cos\theta\sqrt{\beta_m^2 - \beta_i^2}} \quad (1)$$

with $k = 0.94$ (assuming spherical crystals with cubic symmetry), β_m the measured FWHM, β_i the instrumental broadening, determined to 0.07° from a reference sample of a large grained PuO_2 sample annealed at 1200 °C for 30 h. The values presented here are the mean of the three individual results obtained for the diffraction peaks appearing between 40 and 60° (2θ) at constant temperature and given time. Only values of D below 150 nm are considered, because large errors result as β_m approaches β_i.

Eqn (1) assumes that the broadening of the diffraction peaks is contributed by grain size only. In reality, other factors could affect the breadth of a diffraction peak as well, *e.g.* the internal strain of the grains could cause peak broadening. These effects are neglected in our approximation here.

2.4 Grain growth model

The kinetics of growth of the crystallites was modelled according to the classical grain growth model for porous single phase systems eqn (2).[17]

$$D^n = D_0^n + kt \quad (2)$$

D is the grain diameter at time t, D_0 the grain diameter at time $t = 0$, k the grain growth rate constant, which is a function of the temperature:

$$k = k_0\, e^{\left(-\frac{Q}{RT}\right)} \quad (3)$$

R is the gas constant, T temperature, k_0 the kinetic constant, and Q the activation energy of the process which governs the growth of the grain. Fitting was performed using OriginPro 8.1.

3 Results and discussions

PuO_2 nano-crystals were prepared *via* hydrothermal decomposition of Pu-oxalate in water at 95 °C over 4 days.[8] In a first experiment we studied the changes of the crystallite size as a function of the temperature (Fig. 1); the sharpening of the diffraction peaks reflects the particle growth with increasing temperature. Since crystallite growth is significant only above 800 °C, longer term isothermal XRD measurements were performed in the 820–1200 °C interval. The change of the

diffraction patterns over time is shown in Fig. 2 at the example of the measurement at 820 °C (where the changes are minor). Over time a sharpening of the peaks is observed.

We calculated the crystallite size on the basis of the three observed peaks in the window $45° < 2\theta < 60°$ (Table 1, Fig. 2). Since there is some growth during the acquisition period (36 min), the reported values are an average of the size during the acquisition interval.

A modified Williamson–Hall method was applied to quantify the dislocation density in order to measure the grain growth kinetics for nanocrystalline UO_2 in both *in situ* and *ex situ* experiments.[18,19] However, due to experimental limitations in our case the internal strain influence is neglected in our model.

Comparison of the TEM analysis of the original small nanoparticles to its SEM picture of the same material after thermal treatment at 1200 °C for 30 h clearly shows the particles having grown significantly in size from 3.7 ± 1 nm into the micrometer scale (Fig. 3).

It is seen that at constant temperature T the crystallite size increases (Table 1, Fig. 4). The data were fitted with eqn (1) to obtain the grain growth rate constant k as a function of temperature, and the growth exponent n. Given the very fast grain growth rate of nanocrystalline powders, and the time needed for acquisition of a full XRD spectrum (36 minutes), the initial crystallite size at time zero could not be measured. D_0 was thus defined as the first available data point, *i.e.* at 36 min after the beginning of the isotherm. The choice of the exponent n is of critical importance, as it affects greatly the kinetic constant and the activation energy.[20] In order to determine the exponent n, eqn (2) can be rewritten as:

$$D^n - D_0^n = kt \quad (4)$$

By plotting the left side of the equation (eqn (3)) *versus* the time a linear trend is to be expected. The exponent n was chosen as the one giving the best linear fit, by limiting n in the range $n = 2$ to 4. The data between 820 °C and 1000 °C are best fitted with an exponent $n = 4$ or higher, while the data at 1100 °C give an exponent n of 2 (ESI, Fig. S4†). The role of the exponent n and its relevance is discussed later here in more detail.

Only data within the first 6 hours were found to fit eqn (4) well, whereas, during longer-term annealing, crystallite growth proceeds with a slower kinetic. A similar behaviour was however observed by Miao *et al.*[18] for the growth of nanograined UO_2 at 820 °C and 730 °C, and was explained with the grain-growth stagnation mechanism by proposed by Holm.[21] According to this model, a small fraction of slowly moving grain boundaries can effectively pin the faster moving boundaries, and an increase in the temperature is needed for the transition of grain boundaries from low-mobility to the high mobility fraction.

The slope of the linear regression gives the grain growth constant k, reported in Table 2, together with the results of the linear fitting.

Since the data at temperatures of 820 °C, 900 °C, and 1000 °C have the same growth exponent n, the activation energy can be deduced by plotting the logarithm of k as a function of the inverse absolute temperature (Fig. 5). The activation energy for the crystallite growth of nanocrystalline PuO_2 powder in this temperature range was calculated as 351(5) kJ mol^{-1}. This value compares well with the activation energy of 387 kJ mol^{-1} for the grain growth of UO_2 and PuO_2–UO_2 MOX, used in the TRANSURANUS fuel performance code,[23] which also assumes a growth model with an exponent n of 4. Data for the activation energy for grain growth in PuO_2 in powder or bulk were not reported previously.

On the other side the present experiments do not confirm the low activation energy reported in few cases in the literature for the growth of nanocrystalline powder. It has been reported that grain growth in nanocrystalline powders occurs with a reduced activation energy compared to grain growth at a larger scale. For example the activation energy for grain growth in yttria stabilized zirconia nanocrystalline powders was reported to be as low as 13 kJ mol^{-1} (to be compared to 580 kJ mol^{-1} reported for larger grain zirconia).[24] In the current case the activation energy for grain growth in PuO_2 nanocrystal does not appear to be in order of magnitude lower than what could be expected for larger sizes (whereas as discussed data of grain growth in conventional size are lacking). It is important to note

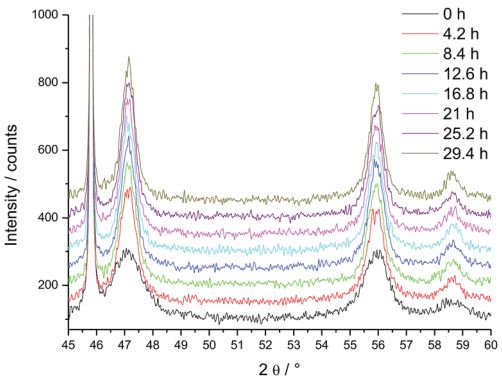

Fig. 2 Evolution of the XRD patterns of PuO_2 as a function of time: change of diffractograms for $45° < 2\theta < 60°$ at constant temperature of 820 °C, repetitive measurement (from bottom to top, time increment in start point of the measurement: 4.2 h). Peak at 45.7° arises from the Pt sample holder.

Table 1 Crystallite size as a function of time at different isothermal temperatures (see Fig. 4, and ESI Fig. S5)

	Crystallite size (nm)			
Time (min)	820 °C	900 °C	1000 °C	1100 °C
36	9.4	19.5	34.5	83.6
72	10.1	21.2	38.4	90.2
108	11.2	22.3	40.2	97.7
144	11.5	23.3	43.3	107.3
180	12.0		45.6	113.0
216	11.8	24.1	46.3	119.7
252	12.3	24.4	48.3	127.2
288	13.1	24.8	48.9	131.4
324	12.8	25.2	49.8	137.2
360		25.7	50.7	142.5

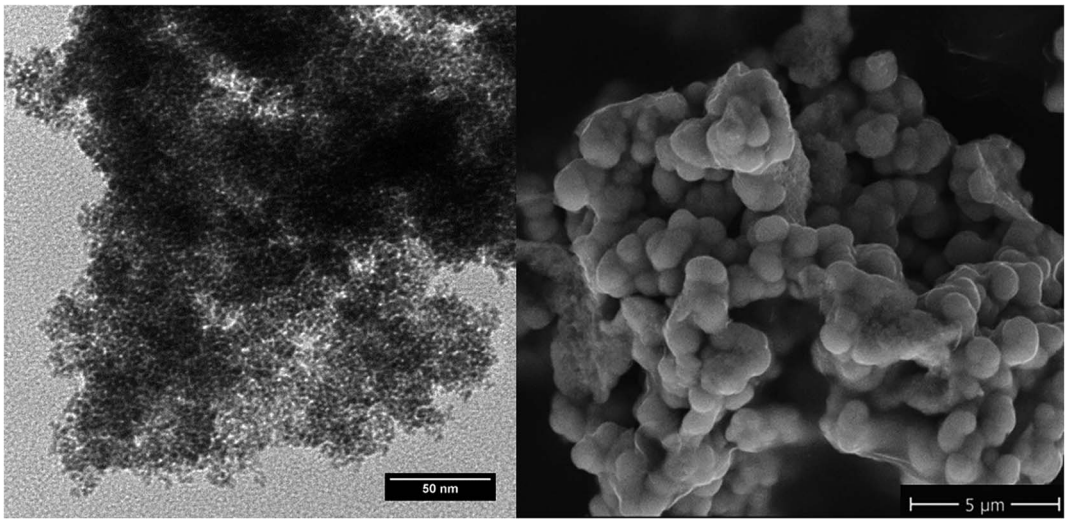

Fig. 3 TEM of the original nanopowder (left) and SEM of powder annealed at 1200 °C for 30 h (right).

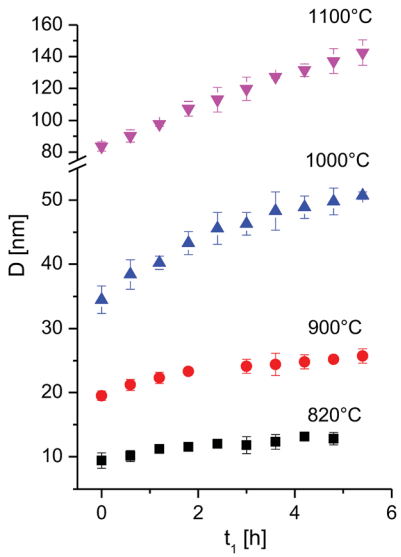

Fig. 4 Crystallite size as a function of time at different isothermal temperatures for the first 6 h. The full time interval is given in Fig. S5.†

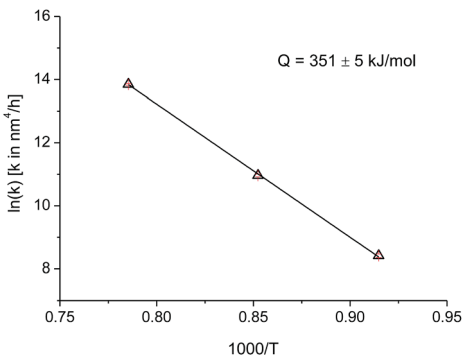

Fig. 5 Arrhenius plot for the grain growth constant k and $n = 4$, for T: 820, 900, 1000 °C.

Table 2 Parameters and results of the linear fitting of the data presented in Fig. S4[a]

Temperature	D_0 [nm]	n	k [nm^n h^{-1}]	R^2
820 °C	9.4	4	4500(250)	0.976
900 °C	19.5	4	57 500(2500)	0.983
1000 °C	34.5	4	1 028 000(25 000)	0.994
1100 °C	83.6	2	2460(20)	0.999

[a] Standard deviation in parentheses.

that in[24] the crystallite data were assumed to have a linear dependency from time ($n = 1$), which can lead to a significant underestimation of the activation energy. A discussion on the importance of the selection of the exponent n on the activation energy is given for example in.[20]

The data allow also for some speculation on the nature of the activation energy derived in the present analysis. According to the Brook model,[22] in a pure system, an exponent of $n = 2$ describes the growth of grain in a dense system. On the other hand, an exponent of n higher than 2 in a pure systems represents the growth of grains in the presence of porosity, where the grains are pinned by the pores and thus the mobility of the pores is the rate controlling mechanism (pore controlled kinetics). According to this model, an exponent n with a value of 4 is observed in systems where pore mobility is controlled by surface diffusion. If this interpretation is accepted, then the calculated activation energy should represent the activation energy for pore mobility governed by surface diffusion. In ionic solids the charge balance requires diffusion of both cations and anions and the rate is limited by the slowest moving specie, being Pu for PuO_2. The activation energy for growth of PuO_2 nanocrystals should thus represent also the activation energy for surface diffusion of Pu in PuO_2. For comparison, a reliable value for the surface diffusion of Pu in PuO_2 could not be found in the literature.

Limited data exist for the activation energy of U diffusion in UO_2. For example Matzke recommended a value of 453 kJ mol^{-1}.[25] This value seems to be high, as the activation energy for surface diffusion is typically lower than the one for grain boundary and volume diffusion. More recent molecular dynamic simulations give a value of the diffusion of U cations on the surface of UO_2 nanocrystals of 299 to 347 kJ mol^{-1}.[26] A study of UO_2 and PuO_2 interdiffusion gives a value of 222 kJ mol^{-1}, assumed to largely due to surface diffusion.[27]

The method we have applied here has some intrinsic limitations that may affect the accuracy of the data. The main limitations are of experimental nature, *e.g.* the need to a fast acquisition time in a short angle range, which limits the applicability of accurate profile analysis, and the choice of the model parameters, above all the time exponent n. It is difficult to assign a precise significance to the exponent n,[20,22] for various reasons: (i) the exponent n might not be an integer as several mechanisms might be concurring, (ii) several values of n could fit with the data with good correlation coefficients, (iii) the data could be fitted also with exponents higher than 4, (iv) the model has been developed for particles separated by nearly spherical isolated pores at the grain boundary, which can differ significantly from the real case.

4 Conclusions

Here for the first time data on the kinetics of the particle growth of PuO_2 are reported; the activation energy is determined to 351(5) kJ mol^{-1} in agreement with data reported for UO_2 and MOX. This first result could represent a preliminary valuable reference for the development of advanced fuel performance code for PuO_2 and MOX.

According to the data on the grain growth of PuO_2 nanocrystals presented here, particle growth proceeds by a pore controlled kinetics mechanism *via* surface diffusion as long as the particles are small or at low temperature (<50 nm, with a growth exponent $n = 4$). At $T = 1100$ °C (when small particles have already agglomerated) the growth mechanism changes to the mechanism of dense material (with $n = 2$). However, the change of the exponent at 1100 °C might as well be addressed to the fact that at this temperature the grain size starts to become comparable to the size of the agglomerates, so that further growth is hindered.

Conflicts of interest

The authors declare no conflict of interest.

Acknowledgements

The authors gratefully acknowledge Oliver Dieste Blanco and Bert Cremer for the microscopic characterisation of the samples. This work was funded by the European Commission, DG JRC and contributes to the Joint Programme on Nuclear Materials (JPNM) of the European Energy Research Alliance (EERA).

Notes and references

1 R. Jovani-Abril, R. Eloirdi, D. Bouëxière, R. Malmbeck and J. Spino, *J. Mater. Sci.*, 2011, **46**, 5.
2 D. Hudry, C. Apostolidis, O. Walter, T. Gouder, E. Courtois, C. Kübel and D. Meyer, *Chem.–Eur. J.*, 2012, **18**, 8283.
3 D. Hudry, C. Apostolidis, O. Walter, T. Gouder, A. Janssen, E. Courtois, C. Kübel and D. Meyer, *RSC Adv.*, 2013, **3**, 18271.
4 D. Hudry, C. Apostolidis, O. Walter, T. Gouder, E. Courtois, C. Kübel and D. Meyer, *Chem.–Eur. J.*, 2013, **19**, 5297.
5 D. Hudry, C. Apostolidis, O. Walter, A. Janßen, D. Manara, J. C. Griveau, E. Colineau, T. Vitova, T. Prüßmann, D. Wang, C. Kübel and D. Meyer, *Chem.–Eur. J.*, 2014, **20**, 10431.
6 R. Jovani-Abril, M. Gibilaro, A. Janßen, R. Eloirdi, J. Somers, J. Spino and R. Malmbeck, *J. Mater. Sci.*, 2016, **477**, 298.
7 V. Tyrpekl, J. F. Vigier, D. Manara, T. Wiss, O. Dieste Blanco and J. Somers, *J. Nucl. Mater.*, 2015, **460**, 200.
8 O. Walter, K. Popa and O. Dieste Blanco, *Open Chem.*, 2016, **14**, 170.
9 L. Balice, D. Bouëxière, M. Cologna, A. Cambriani, J.-F. Vigier, E. De Bona, D. G. Sorarù, C. Kübel, O. Walter and K. Popa, *J. Nucl. Mater.*, 2018, **498**, 307.
10 K. Popa, O. Walter, O. Dieste Blanco, A. Guiot, D. Bouëxière, J.-Y. Colle, L. Martel, M. Naji and D. Manara, *CrystEngComm*, 2018, **20**, 4614.
11 N. Vaida and C.-K. Kim, *J. Radioanal. Nucl. Chem.*, 2010, **284**, 341.
12 N. Xu, D. Gallimore, E. Lujan, K. Garduno, L. Walker, F. Taylor, P. Thompson and L. Tandon, *J. Radioanal. Nucl. Chem.*, 2016, **307**, 1203.
13 B. Arab-Chapelet, P. M. Martin, S. Costenoble, T. Delahaye, A. C. Scheinost, S. Grandjean and F. Abraham, *Dalton Trans.*, 2016, **45**, 6909.
14 R. Taylor, *Reprocessing and recycling of spent nuclear fuel*, Woodhead Publishing, 2015.
15 P. Govindan, A. Palamalai, K. S. Vijayan, M. Raja, S. Parthasarathy, S. V. Mohan and R. V. Subba Rao, *J. Radioanal. Nucl. Chem.*, 2000, **246**, 441.
16 C. E. Zvoriste-Walters, S. Heathman, R. Jovani-Abril, J. L. Spino, A. Janssen and R. Caciuffo, *J. Nucl. Mater.*, 2013, **435**, 123.
17 M. N. Rahaman, *Ceramic Processing and Sintering*, 2nd edn, Taylor and Francis, 2003, p. 602.
18 Y. Miao, T. Yao, J. Lian, J.-S. Park, J. Almer, S. Bhattacharya, A. M. Yacout and K. Mo, *Scr. Mater.*, 2017, **131**, 29.
19 T. Yao, K. Mo, D. Yun, S. Nanda, A. M. Yacout and J. Lian, *J. Am. Ceram. Soc.*, 2017, **100**, 2651.
20 L. Bourgeois, Ph. Dehaudt and C. Lemaignan, *J. Nucl. Mater.*, 2001, **295**, 73.
21 E. A. Holm and S. M. Foiles, *Science*, 2010, **328**, 1138.
22 R. J. Brook, *Treatise on materials science and technology*, ed. F. J.Wang, 1976, vol. 9, pp. 331–363.
23 P. Van Uffelen, P. Botazzoli, L. Luzzi, S. Bremier, A. Schubert, P. Raison, R. Eloirdi and M. A. Barker, *J. Nucl. Mater.*, 2013, **434**, 287.

24 S. Shukla, S. Seal, R. Vij and S. Bandyopadhyay, *Nano Lett.*, 2003, **3**, 397.
25 H.-J. Matzke, *J. Chem. Soc., Faraday Trans.*, 1990, **86**, 1243.
26 A. S. Boyarchenkov, S. I. Potashnikov, K. A. Nekrasov and A. Ya Kupryazhkin, *J. Nucl. Mater.*, 2013, **442**, 148.
27 R. Verma and P. R. Roy, *Proceedings of the symposium on surface and interface properties in materials science [held at] Roorkee, October 13–15*, 1980.